Journal of Materials Chemistry A

RSC Publishing

PAPER

View Article Online
View Journal | View Issue

Cite this: J. Mater. Chem. A, 2013, 1, 14692

High-performance pyrolyzed iron corrole as a potential non-precious metal catalyst for PEMFCs†

Hsin-Chih Huang,[a] Chen-Hao Wang,*[a] Indrajit Shown,[b] Sun-Tang Chang,[a] Hsin-Cheng Hsu,[a] He-Yun Du,[b] Li-Chyong Chen[c] and Kuei-Hsien Chen*[bc]

Received 4th September 2013
Accepted 8th October 2013

DOI: 10.1039/c3ta13515b

www.rsc.org/MaterialsA

This work demonstrates the performance of carbon black-supported pyrolyzed Fe–corrole (py-Fe–corrole/C) as a cathode catalyst for the oxygen reduction reaction (ORR) in PEMFCs. The ORR measurements reveal that the py-Fe–corrole/C exhibits good ORR activity, *via* the direct four-electron reduction pathway, in the reduction of O_2 to H_2O. The H_2–O_2 PEMFC produces high activity and good stability. The enhanced ORR activity is attributable to the network structure of poly-aromatic hydrocarbons, the quaternary (graphitic)-type nitrogen and the coordination structure of the py-Fe–corrole/C. Square wave voltammetry has been applied to the py-Fe–corrole/C to perform a redox reaction of Fe(II)/Fe(III) at 0.6 V. Finally, detailed *in situ* X-ray adsorption spectroscopy has been applied to determine the ORR mechanism of py-Fe–corrole/C.

Introduction

A proton exchange membrane fuel cell (PEMFC) is a power source to convert the chemical energy in fuel and oxidant to electricity. The core unit of the PEMFC, a membrane-electrode-assembly (MEA), is a polymer electrolyte membrane that is sandwiched between an anode and a cathode. To speed up the redox reaction, a high loading of platinum catalyst is employed in the anode and the cathode. Since the oxygen reduction reaction (ORR) of the cathode is much slower than the hydrogen oxidation reaction of the anode, the loading of the Pt catalyst in the cathode is much higher than that of the anode, making the PEMFC expensive. To reduce the cost of the PEMFC, non-precious metal catalysts for the ORR are extremely important, and have attracted substantial attention in recent years.

Recently, Liu *et al.* used an iron–nitrogen-doped graphene–carbon composite catalyst to suppress the agglomeration, protecting the catalytic active sites that are located on the surface of graphene sheets. The electron transfer number for the ORR exceeded 3.97 and the corresponding H_2O_2 yield was below 1.5%, approaching to that of Pt/C.[1] In 2013, Hu *et al.* synthesized self-supported and preserved nanoworm-shaped non-precious metal catalysts using pre-prepared polyaniline nanofibers as the nitrogen and carbon precursors. A significant enhancement in the intrinsic activity and onset potential for the ORR is observed as the Fe content in the precursor is increased, with an electron transfer number of approximately 3.99.[2] Oh *et al.* found that transition metals serve to catalyze the formation of active nitrogen functional groups for the ORR by doping nitrogen into carbon. Improving the activity and durability of nitrogen-modified carbon-based catalysts is important. The Co–ED (ethylenediamine)/PPy (polypyrrole)–CNF in the cathode of an H_2–O_2 PEMFC test delivered a maximum power density of approximately 280 mW cm^{-2}, with no significant degradation over at least 100 hours.[3] Zhang *et al.* synthesized a non-precious catalyst by pyrolyzing a carbon-supported iron and cobalt triethylenetetramine binary metal chelate at high temperature (FeCoTETA/C). The electron-transfer number and the yield of H_2O_2 during the ORR with the rotating-ring disk electrode (RRDE) are calculated to be approximately 3.8 and 10%. An H_2–O_2 PEMFC based on this cathode catalyst yielded a maximum output power density of 256 mW cm^{-2}.[4] Zhao *et al.* used a pyrolyzed iron imidazolate framework that was mixed with a zinc imidazolate framework (FeIM/ZIF-8) with non-platinum group metals as cathode catalysts. The PEMFC test in H_2–O_2 revealed a maximum power density of 287 mW cm^{-2}.[5]

Chang *et al.* studied the use of pyrolyzed cyanocobalamin (vitamin B12), supported by carbon black (py-B12/C), as a catalyst for the ORR in PEMFCs.[6] Based on analysis calculations, they suggested that py-B12 with a Co–corrin structure with a low symmetry follows a preferable ORR path, which is not followed by the porphyrin with a highly symmetric structure. According to this idea, a similar structure of Co–corrole with low symmetry has been synthesized for ORR.[7] It yielded an output power of 275 mW cm^{-2} with a lower catalyst loading than that achieved in previous studies of Co-based catalysts for PEMFCs. Corrole is a tetrapyrrolic

[a]Department of Materials Science and Engineering, National Taiwan University of Science and Technology, Taipei 10607, Taiwan. E-mail: chwang@mail.ntust.edu.tw
[b]Institute of Atomic and Molecular Science, Academia Sinica, Taipei 10617, Taiwan. E-mail: chenkh@pub.iams.sinica.edu.tw
[c]Center for Condensed Matter Sciences, National Taiwan University, Taipei 10617, Taiwan

† Electronic supplementary information (ESI) available. See DOI: 10.1039/c3ta13515b

macrocyclic compound with one carbon atom fewer than porphyrin. Many non-precious metal catalysts based on the ligand behavior of corrole have been discussed in the pursuit of increased and prolonged ORR activity.[8–12]

The central metal ion of the macrocycle seems to play an important role in oxygen reduction. Fe and Co metal ion centers have been found to display excellent electrocatalytic properties attributable to their distinct redox properties and these have been proposed as active sites for the ORR.[13–17] The nature of the ligand–metal interaction also plays an important role in the ORR activity of these compounds. In particular, high ionization potential of the metal ion centers has been considered to be an important factor influencing ORR activity.[18–20] With respect N_4-chelates, iron-based complexes have been found typically to catalyze the ORR through a four-electron reduction pathway to produce water, while cobalt complexes catalyze a two-electron reduction pathway.[13,14,21,22] Alt *et al.* further explained this activity using molecular orbital (MO) theory based on oxygen adsorption.[23] Studies of the ORR activity and durability of the non-precious metal catalysts have been reviewed.[15,17,24–27] Many species, including the transition metal nitrogen-containing complexes, types of transition metals, catalyst loading, surface properties of carbon support and nitrogen content, affect the characteristics of the ORR.

This work elucidates a simple method for synthesizing pyrolyzed Fe–corrole that is supported by carbon black (py-Fe–corrole/C) for application to fuel cells. The py-Fe–corrole/C catalyst exhibits higher catalytic activity in the ORR by the direct four-electron reduction pathway than do other iron-containing macrocyclic compounds, such as porphyrin, phthalocyanine, and tetraazannulene. This study investigation will compare the ORR performance with the py-Fe–corrole/C with that achieved in previous studies of py-Co–corrole/C.

Experimental

General procedure for synthesis of 5,10,15-triphenyl corrole

The synthesis of 5,10,15-triphenyl corrole herein was based on the method of Koszarna *et al.*, with some modifications. Pyrrole (16 mmol) and benzaldehyde (8 mmol) were dissolved in 320 ml of a water–methanol (1 : 1) mixture, which was stirred for 5 min in an atmosphere of argon, before concentrated HCl (0.8 mmol) was added.[28] The reaction mixture was then stirred for another 3 h. The organic layer was separated using $CHCl_3$, washed twice with water, dried (Na_2SO_4), filtered and diluted to 600 ml $CHCl_3$. DDQ (8 mmol) was added to the solution and refluxed for 1.5 h in an atmosphere or argon. The extent of the reaction was monitored by TLC. The reaction mixture was filtered through a small column of silica. The solvent was then removed under a vacuum, and the residue was dissolved in CH_2Cl_2. Column chromatography over SiO_2 (CH_2Cl_2/hexane, 2 : 1) gave purified 5,10,15-triphenyl corrole (605 mg, 43.4%).

Synthesis of (nitrosyl) (5,10,15-triphenyl corrolato) iron(III)

Insertion of Fe(III) following the procedure in the literature: 5,10,15-triphenyl corrole (0.4 mmol) was dissolved in pyridine/ethanol (1 : 2) under dinitrogen and mixed with $FeCl_2 \cdot 4H_2O$ (1.5 mmol) for 3 h at room temperature, after which 1 ml saturated $NaNO_2$ was added and the solution was stirred under dinitrogen for 30 min at room temperature.[29] Finally, the solvent was evaporated and passed through a silica column with CH_2Cl_2/Hex (1 : 3). Recrystallization with CH_2Cl_2/CH_3OH gave purified (nitrosyl) (5,10,15-triphenyl corrolato) iron(III) in 41% yield (130 mg).

Preparation of pyrolyzed Fe–corrole and pyrolyzed Fe–corrole/C

The final catalyst was prepared according to the following procedure. A 0.10 g mass of Fe–corrole was dissolved in 10 mL of tetrahydrofuran (THF, 99.7%, Alfa Aesar) with stirring for 30 minutes at room temperature. Then, 0.40 g of carbon black (Vulcan XC-72R) was added to the Fe–corrole solution, which was stirred for 30 minutes at room temperature. The mixture was heated using steam to 80 °C to eliminate the solvent. The suspension was filtered through filter paper to obtain a slurry, which was dried at room temperature under vacuum for 12 hours.

The pyrolyzed Fe–corrole, supported by carbon black, was prepared at 700 °C. The formed compound was py-Fe–corrole/C-700. In the common pyrolysis process, the slurry was loaded into a fused aluminum oxide boat, which was introduced into a furnace in a quartz tube; the specific temperature was increased at a rate of 20 °C per minute in an atmosphere of nitrogen, in which it remained for 2 h. Following the pyrolysis, the furnace was cooled to room temperature by natural convection. For example, at the pyrolysis temperature of 700 °C, the mass of py-Fe–corrole/C was 0.42 g, representing a total weight loss of approximately 16% throughout the process. The Fe–corrole solution without added carbon black was loaded into a silica boat for pyrolysis, yielding py-Fe–corrole, to be analyzed by Raman spectroscopy, X-ray photoelectron spectroscopy (XPS) and X-ray absorption spectroscopy (XAS).

Preparation of py-FePc/C and Fe/C

The pyrolyzed iron(II) phthalocyanine/C (py-FePc/C) and the Fe/C were prepared to compare their electrochemical activities with those of py-Fe–corrole. The py-FePc/C was prepared as follows: 0.1 g of iron(II) phthalocyanine (FePc, 99%, Acros) and 0.4 g of carbon black (Vulcan XC-72R) were dispersed in tetrahydrofuran (THF, 99.7%, Alfa Aesar) solution, which underwent 30 minutes of ultrasonication to form a homogeneous solution. Thereafter, the mixture was heated using steam to 80 °C to eliminate the solvent. The suspension was filtered through filter paper to obtain the slurry, which was dried at room temperature under a vacuum for 12 hours. Finally, the pyrolysis process was used to prepare the py-FePc/C at 700 °C. The mass of the as-prepared py-FePc/C was 0.425 g, representing a total weight loss of approximately 15.0% throughout the process. Similarly, in the preparation of Fe/C, 0.29 g of dried iron(III) chloride ($FeCl_3$, 98%, Acros) and 0.4 g of carbon black (Vulcan XC-72R) were dispersed in de-ionized water and the above py-FePc/C preparation process was then implemented. In the final step, the

catalyst mixture was pyrolyzed in an atmosphere of 5% hydrogen at 200 °C for 2 hours.

Material analysis

A Raman spectrum was recorded using a Jobin-Yvon LabRAM HR800-Confocal micro-Raman spectroscope with a 633 nm He–Ne laser as the excitation source. X-ray photoelectron spectroscopy (XPS, VG ESCA Scientific Theta Probe) using 1486.6 eV Al Kα source was used to study the changes of the N1s of the pyrolyzed Fe–corrole. The X-ray absorption near-edge structure (XANES) at the Fe K-edge was recorded at beam line 17C1, which is based on a multi-pole wiggler source with a critical energy of 2.7 keV. The electron storage ring was operated at an energy of 1.5 GeV with a beam current of 120–200 mA. The beam line employs a double Si(1 1 1)-crystal monochromator for energy selection with a resolution ($\Delta E/E$) of better than 2×10^{-4} in the energy range 5–15 keV. All spectra were obtained at room temperature in transmission mode, and the intensities of the incident and transmitted X-ray beams were measured using gas-filled ionization chambers. The catalyst powder was pressed into a slot of a stainless-steel holder and then placed in a cell for treatment under the desired conditions. The standard material, iron foil, was measured simultaneously in the third ionization chamber to enable energy calibration scan by scan. The *in situ* Fe K-edge XAS measurements were made at the same beam line 17C1 and in a three-compartment cell using a potentiostat/galvanostat instrument (Metrohm Autolab). The catalyst with Nafion® solution was hand-painted onto the 0.25 cm^2 gold net working electrode. The counter electrode and reference electrode were Pt foil and a saturated calomel electrode (0.242 V *vs.* NHE), respectively. All potentials in this work are with reference to the reversible hydrogen electrode (RHE). The electrolyte was oxygen-saturated 0.1 M $HClO_4$ solution. The XANES data were processed involving background subtraction, normalization with respect to the edge jump, Fourier transformation, and curve fitting, in the IFEFFIT software package. The theoretical phase shifts and backscattering amplitudes for particular atom pairs were calculated using the FEFF7 code.[30]

Electrochemical measurements

All electrochemical measurements were made in a three-compartment cell using a potentiostat/galvanostat instrument (Biologic Bi-stat). The working electrode was an RRDE (PINE AFE7R9GCPT) with a glassy carbon (GC) disk and a ring made of platinum. The counter electrode and reference electrode were Pt foil and a saturated calomel electrode (0.242 V *vs.* NHE), respectively. All potentials in this work are with reference to the reversible hydrogen electrode (RHE). The electrolyte that was used in all electrochemical measurements was oxygen-saturated 0.1 M $HClO_4$ solution.

Catalyst ink was prepared by mixing 160 mg of catalyst with 20 mL deionized water. 20 μL of the ink and 5 μL of 0.1 wt% Nafion® solution were dropped onto the GC disk, which was then left to dry in air at room temperature. Before the catalyst ink was deposited onto the GC disk, the GC disk had been polished to a mirror-like finish using 1.0 and then 0.05 μm alumina slurry. Cyclic voltammetry was performed on the catalysts at the specified scan rates. The ORR curves at the GC were plotted at a low scan rate of 10 mV s^{-1} to reduce the substantial non-Faradic current that would otherwise have been produced by the catalysts. To determine the yield of hydrogen peroxide in the ORR that was catalyzed by the catalysts on the GC disk, 1.2 V *vs.* RHE was applied to the ring to generate a current that oxidized the hydrogen peroxide. For square wave voltammetry, the curve for the GC was obtained at a step potential of −5 mV, an amplitude of −20 mV and a scan frequency of −10 Hz.

Fuel cell test

A membrane-electrode-assembly (MEA) with an area of 5 cm^2 was made by hot-pressing two electrodes on both sides of a Nafion® 212 (H^+, DuPont) at 135 °C and 130 kg cm^{-2} for 2 min. In the preparation of the specific cathode, the py-Fe–corrole/C was dispersed in a 5 wt% Nafion® solution as a cathode catalyst ink, with a catalyst-to-dry Nafion® mass ratio of 1 : 2. The cathode catalyst ink was hand-painted onto the carbon cloth, giving a py-Co–corrole/C loading of approximately 2.0 mg cm^{-2}, and the cathode was then dried at room temperature in a vacuum for 6 hours. The anode of MEA was a commercial electrode (E-TEK)–Pt/C with a metal loading of 0.25 mg cm^{-2}. A polarization experiment was carried out on the PEMFC at 70 °C, using hydrogen and oxygen through the anode and the cathode at flow rates of 0.1 and 0.15 slpm. Hydrogen and oxygen were passed through the humidifiers at 70 °C before they entered an MEA. The back pressure gauges on the anode and the cathode sides were set to 1 atm. The PEMFC performance was measured using a fuel-cell test station (Asia Pacific Fuel Cell Technologies, Ltd.) by recording the cell voltage and current after they had reached steady values.

Results and discussion

The ORR pathway involves mainly the following reactions.

$$O_2 + 4H^+ + 4e^- \rightarrow 2H_2O,\ E^0 = 1.229\ V \quad (1)$$

$$O_2 + 2H^+ + 2e^- \rightarrow 2H_2O_2,\ E^0 = 0.695\ V \quad (2)$$

$$H_2O_2 + 2H^+ + 2e^- \rightarrow H_2O,\ E^0 = 1.763\ V \quad (3)$$

H_2O_2 may also chemically decompose into O_2 and H_2O.

Reaction (1) follows a direct reduction pathway that involves a four-electron transfer. Reaction (2) follows an H_2O_2 pathway that involves a two-electron transfer. Since a direct ORR pathway yields a higher thermodynamically reversible potential than an H_2O_2 pathway, reaction (1) is preferable to reaction (2) as the ORR in the PEMFC.

When the macrocyclic/transition metal complexes ($M–N_4$ moieties, M: Co and Fe) are pyrolyzed at a particular temperature, their structures are partially or completely destroyed, resulting in new active sites that have greater and more stable ORR activity than the untreated $M–N_4$ moieties. Fig. 1a presents the ORR behaviors of py-Fe–corrole/C, py-FePc/C and Fe/C, as

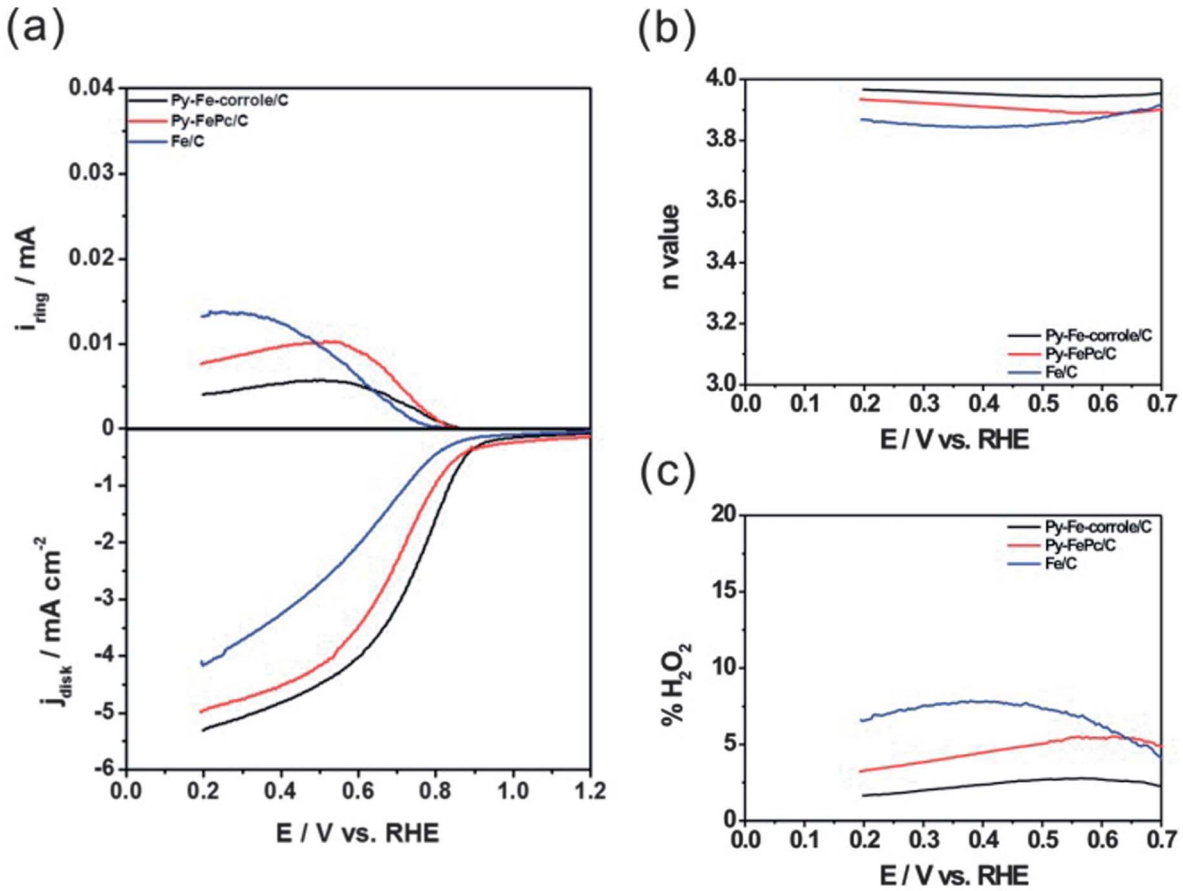

Fig. 1 (a) ORR curves for py-Fe–corrole/C, py-FePc/C and Fe/C; (b) the *n* values and (c) %H_2O_2 of the catalysts dependence on disk potentials. Rotating speed: 1600 rpm; scan rate: 10 mV s^{-1}; ring potential: 1.2 V.

determined by the RRDE method. The lower and upper parts of Fig. 1a plot the density of the disk current (J_d) and the ring current (I_r), respectively, as functions of the applied potential. The typical ORR curve obtained in acidic media comprises three dominant potential regions – the kinetic range (>0.8 V), the mixed range (0.8–0.6 V), and the mass-transfer range (<0.6 V). The py-Fe–corrole/C outperforms the py-FePc/C and the Fe/C in all potential regions, indicating that the py-Fe–corrole/C has a much higher ORR activity. The nominal Fe wt% in the py-Fe–corrole/C, the py-FePc/C and the Fe/C is 0.95%, 1.74% and 20%, respectively. The fact that the py-Fe–corrole/C has the lowest Fe loading and yet exhibits the highest ORR activity attests to its superb catalytic activity. At a pyrolysis temperature of 700 °C, the py-Fe–corrole/C exhibited the optimal performance with the highest J_d and the lowest I_r. The total electron-transfer number (n) and the hydrogen peroxide yield (%H_2O_2) in the ORR can be derived from eqn (4) and (5):

$$n = \frac{4I_d}{I_d + \frac{I_r}{N}} \quad (4)$$

$$\%H_2O_2 = \frac{\frac{2I_r}{N}}{I_d + \frac{I_r}{N}} \times 100\% \quad (5)$$

where N is the RRDE collection efficiency, which was determined to be 0.37 herein. Fig. 1b and c plot the electron-transfer number (n value) and the hydrogen peroxide yield (%H_2O_2) during the ORR, respectively, as functions of the potential of the glassy carbon (GC) disk. At a large overpotential of 0.3 V, the n values for the py-FePc/C and the Fe/C are reduced to 3.90 and 3.80, respectively. However, for the py-Fe–corrole/C, the n values and %H_2O_2 remain at approximately 3.97 and 1.5%, respectively, over a wide range of overpotentials up to 0.7 V, indicating that the ORR of py-Fe–corrole/C proceeds preferentially along the four-electron direct ORR pathway.

Fig. 2 presents the Raman spectra of pristine Fe–corrole and py-Fe–corrole. After the pyrolysis, py-Fe–corrole exhibits two strong peaks at 1330 and 1580 cm^{-1}, which are the D- and G-peaks, respectively, of the carbon-like materials, suggesting that py-Fe–corrole forms a network structure of poly-aromatic hydrocarbons. The formation of graphite-like carbon may enhance the electronic conductivity and corrosion resistance of the catalysts.[31,32]

Fig. 3a and b present XPS N1s spectra of pristine Fe–corrole and py-Fe–corrole, respectively, with the corresponding fitting results in Table 1. The XPS spectrum of the pristine Fe–corrole includes peaks of pyridinic-type and pyrrolic-type nitrogen at 398.5 and 400.4 eV, respectively. After the pyrolysis, part of pyridinic-type and pyrrolic-type nitrogen still exist, but the rest

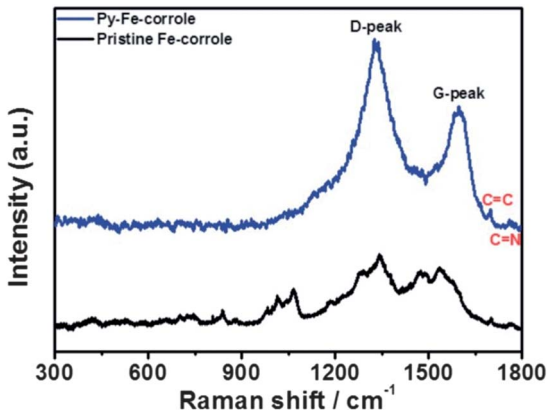

Fig. 2 Raman spectra of py-Fe–corrole and pristine Fe–corrole.

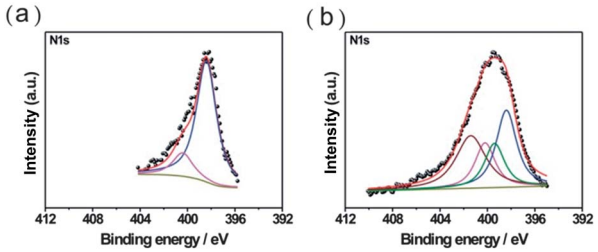

Fig. 3 XPS showing N1s spectra of (a) prisitine Fe–corrole and (b) py-Fe–corrole.

Table 1 The fitting results from XPS N1s spectra of Fig. 3

N1s (atomic %)	Quaternary-type nitrogen (401.4 eV)	Pyrrolic-type nitrogen (400.3 eV)	Cyanide (399.4 eV)	Pyridinic-type nitrogen (398.5 eV)
Pristine Fe–corrole	—	38.5%	—	61.5%
Py-Fe–corrole	32.0%	18.0%	18.0%	32.0%

of species are converted to cyanide and quaternary-type nitrogen, which are responsible for the peaks at 399.4 eV and 401.4 eV, respectively.[33,34] Chung *et al.* proposed that the quaternary-type nitrogen lowers the carbon band gap energy and possibly promote catalytic activity.[35] Liu *et al.* also proposed that quaternary-type nitrogen is less susceptible to protonation in the acidic environment, explaining the high stability after pyrolysis.[36] Recently, studies of nitrogen-doped carbon catalysts have reported that graphitic (quaternary) nitrogen exhibits ORR catalytic activity.[37–40] The central iron-containing corrole ring in Fe–corrole that is pyrolyzed at a high temperature is partially destroyed, resulting in a new catalytic site that has a very high ORR activity and stability. From N1s of the XPS spectra, pyrolysis changes the binding energies, indicating that the interaction between iron and the N_4-chelate changes the profile of the adsorbed/desorbed energies of O_2, enhancing the ORR activity.

Fig. 4 plots the polarization curves of PEMFCs using the py-Fe–corrole/C and the py-FePc/C in the cathodes. The figure reveals that the py-Fe–corrole/C performs much better than the

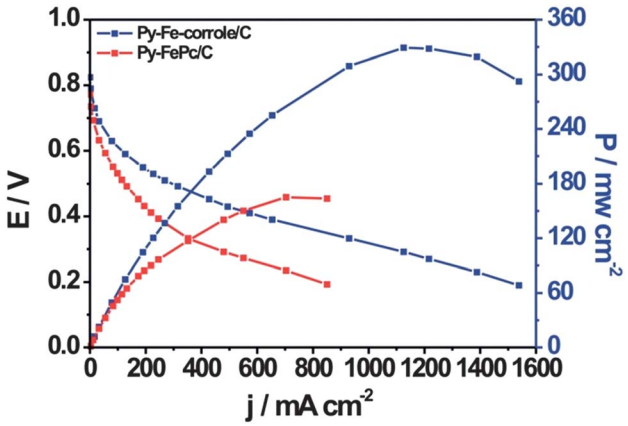

Fig. 4 Polarization curves of the H_2–O_2 PEMFCs using py-Fe–corrole/C and py-FePc/C as the cathodes. Operation temperature: 70 °C; back pressure of H_2 and O_2: 1 atm; anode catalyst: 0.25 mg cm^{-2} of Pt/C; cathode catalyst: 2.0 mg cm^{-2} of specific catalyst; electrolyte: Nafion® 212 (H^+, DuPont).

py-FePc/C. The maximum power density of 330 mW cm^{-2} that is obtained using the py-Fe–corrole/C is twice of that obtained using the py-FePc/C. The 100-hour durability test of PEMFCs is performed using the py-Fe–corrole/C at 0.4 V with flowing H_2 and air fed into the anode and the cathode, respectively, as presented in Fig. 5. The current density decays by approximately 25% in 100 hours. The reason for this degradation is unclear. However, if the cathode is purged by nitrogen gas at a high flow rate after 100 hours of operation, then the performance of py-Fe–corrole/C PEMFCs can be recovered to just 1–2% below the initial value. Water flooding seemingly occurred in the cathode during the durability test, resulting in the degradation.

Fig. 6 presents the Fe XANES spectra of pristine Fe–corrole, py-Fe–corrole and pristine FeTMPPCl, indicating the Fe oxidation state of 3+ for all of the samples. Interestingly, pyrolysis does not change the oxidation state of Fe in Fe–corrole.

The coordination kinetics of the adsorption of O_2 by the M–N_4 catalysts in the ORR are not fully understood. The four

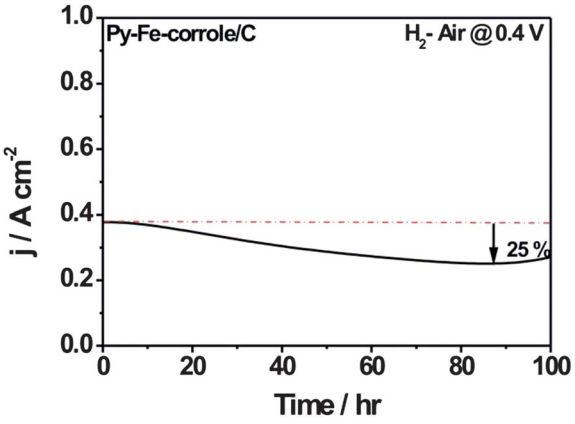

Fig. 5 The 100-hour durability test of H_2–O_2 PEMFC using py-Fe–corrole/C. Operation conditions: H_2-Air, 70 °C and 1 atm of back pressure. Operation temperature: 70 °C; back pressure of H_2 and air: 1 atm; anode catalyst: 0.25 mg cm^{-2} of Pt/C; cathode catalyst: 2.0 mg cm^{-2} of py-Fe–corrole/C; electrolyte: Nafion® 212 (H^+, DuPont).

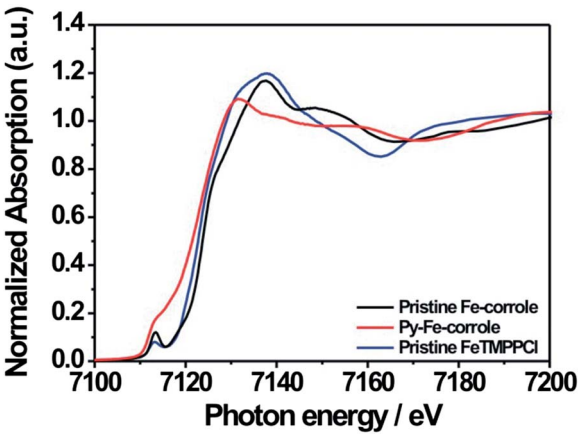

Fig. 6 XANES spectra of pristine Fe–corrole, py-Fe–corrole and pristine FeTMPPCl.

major available models of the adsorption of O_2 onto catalysts are Griffith's model, the Pauling model, the *trans*-Yeager model and the *bridge*-Yeager model.[14] The latter two predict four-electron transfer, and the *trans*-Yeager model is well accepted for platinum catalysts, while the *bridge*-Yeager model is widely accepted for macrocyclic compound catalysts. The Fe-containing corrole ring participates in the ORR. When the Fe–NO bond of the iron-containing corrole is cleaved by pyrolysis, the vacant site coordinates easily with O_2. Studies of other M–N_4 moieties in the ORR yielded similar results, in which the M–N_4 moieties were partially or completely decomposed in pyrolysis.[41,42]

The oxidation state of the transition metal, the redox potential of M(II)/M(III) and the ligand effect dominate the ORR activity of the Fe-based and Co-based macrocyclic compounds.[14,19] However, cyclic voltammetry of the pyrolyzed catalysts does not yield useful information since, in most cases, after heat treatment, the Faradaic currents will be overwhelmed by the carbon-like capacitance.[43] To overcome this limitation, Ramaswamy and Mukerjee used square wave voltammetry (SWV) to study the evolution of active sites in the catalysts.[44] Fig. 7 plots the SWV curve of py-Fe–corrole/C in N_2-saturated 0.1 M $HClO_4$, and the redox transition that involves the central metal Fe(II)/Fe(III) is observed at 0.6 V.

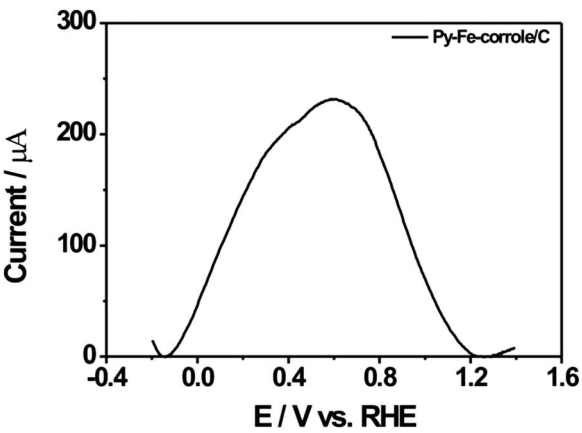

Fig. 7 Square wave voltammetry of py-Fe–corrole/C in 0.1 M $HClO_4$. Step potential: −5 mV; amplitude: −20 mV; scan frequency: −10 Hz.

The delta-mu ($\Delta\mu$) curve, obtained by subtracting the XANES signatures according to $\Delta\mu = \mu(0.90\ V) - \mu(0.30\ V)$, is a surface-sensitive technique used to remove the signal of the bulk, allowing direct spectroscopic probing of the surface adsorbates on a catalyst that is being used by the *in situ* measurement. This technique facilitates understanding of the relationship among adsorption sites, the catalyst surface structure and electrochemical potential.[44–49] Fig. 8 presents the *in situ* XANES spectra of py-Fe–corrole at two potentials of 0.3 V and 0.9 V. At 0.3 V, the central metal is in the reduced Fe(II) state with no adsorbate at the axial position, while at 0.9 V, the central metal is oxidized to the Fe(III) state with an oxygen atom at the axial position.

In the delta-mu spectra in Fig. 8, the positive peak indicates the difference between the probability of absorption at the pre-edge energy. This difference is attributable to the central metal undergoing a transition from the Fe(II)–N_4-coordinated species to the O–Fe(III)–N_4 coordinated species. It reveals that the central Fe(II) metal that is bonded to four nitrogen atoms is the active site that binds oxygen in the axial position, and that the redox transition from Fe(III) to Fe(II) triggers the adsorption of oxygen by the mechanism by which the metal chelates of the N4-type catalyze the reduction of oxygen.[19]

Regarding the mechanism of the activity of the above iron-based macrocyclic catalyst, Schulenburg *et al.* proposed a model of the structure of the active site.[50] For geometrical reasons, more than four nitrogen atoms are unlikely to coordinate to an Fe(III) center, because the nitrogen ligands are already bonded

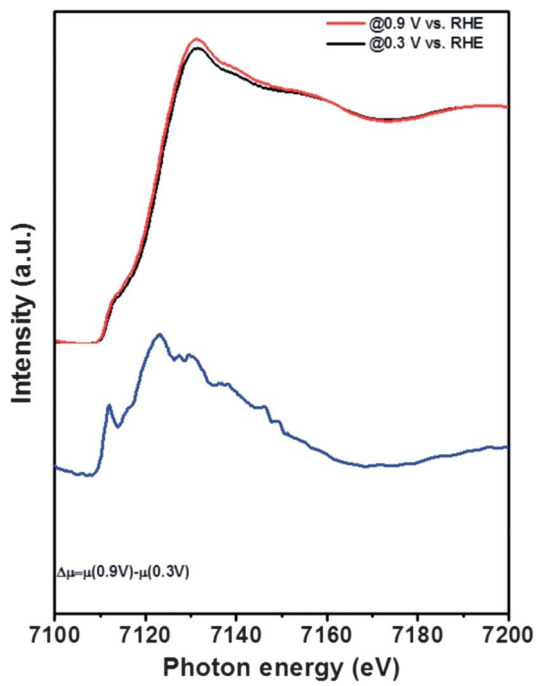

Fig. 8 Experimental XANES and delta-mu curve of py-Fe–corrole. Delta-mu curves were obtained by subtracting the XANES signatures according to $\Delta\mu = \mu(0.90\ V) - \mu(0.30\ V)$. Experiments were collected at Fe K edges under *in situ* conditions in N_2-saturated 0.1 M $HClO_4$ solution.

in the graphene layers. The missing ligands can be adsorbed by the oxygen or interact with a neighboring graphene layer. Based on ToF-SIMS measurements of a pyrolyzed FeTMPP–Cl catalyst, Lefevre *et al.* proposed that FeC_xN_y is responsible for the catalytic activity.[51,52] Bron *et al.* and Bouwkamp-Wijnoltz *et al.* have suggested that FeN_x sites contribute to the ORR activity, and they identified the coordination of iron with 3 or 4 nitrogen atoms by making EXAFS measurements.[53,54] Ziegelbauer *et al.* used *in situ* EXAFS to confirm direct spectroscopic observations of the geometry of O_{ads} on active sites of pyropolymer. The specific geometrical adsorption of molecular oxygen relative to the plane of the $M–N_x$ moieties strongly influences the oxygen reduction reaction pathway.[49]

To obtain more information about the structure and mechanism of the adsorption of molecular oxygen on py-Fe–corrole with a central metal during the ORR of py-Fe–corrole, Fig. 9 presents the Fourier transforms of the *in situ* Fe K-edges EXAFS measurements during the ORRs with scanning from 1.2 V to 0.3 V, and Table 2 presents the fitting results of Fe–N bonding lengths at various potentials. The original Fe–N bond length is 1.95 Å, which varies with the applied potential. At 1.2–0.9 V, the Fe–N bond length is elongated to 2.03–2.02 Å, indicating that oxygen was adsorbed onto py-Fe–corrole and had started to react. At 0.6 V, the Fe–N bond length reaches its maximum of 2.15 Å. Both oxygen and electrons were in a mixed state for ORR. The redox transition involved the central metal Fe(II)/Fe(III) from SWV, which effectively dominated the ORR activity. Electrochemical and standard EXAFS analysis revealed that 0.3 V was the "cleanest" (adsorbate-free) potential.[49] In the mass transfer process, the oxygen was desorbed from py-Fe–corrole and the Fe–N bond length recovered to 1.93 Å.

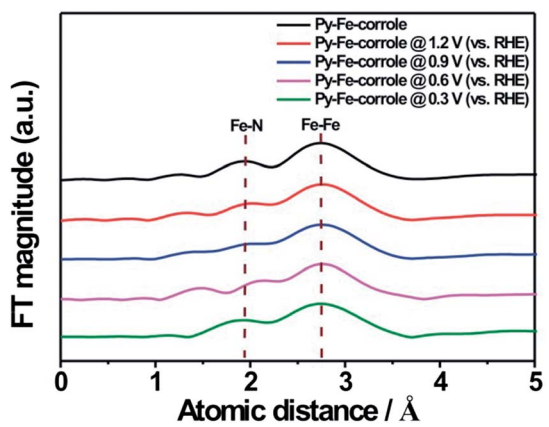

Fig. 9 Fourier transforms of *k*3-weighted EXAFS data at the Fe K-edge for py-Fe–corrole at different potentials in 0.1 M $HClO_4$ solution.

Table 2 The Fe–N distances from *in situ* EXAFS data of Fig. 9

Catalyst	Fe–N distance/Å
Py-Fe–corrole	1.95
Py-Fe–corrole @ 1.2 V	2.03
Py-Fe–corrole @ 0.9 V	2.02
Py-Fe–corrole @ 0.6 V	2.15
Py-Fe–corrole @ 0.3 V	1.93

Conclusions

The py-Fe–corrole/C exhibits good electrochemical ORR activity and is a candidate catalyst for use in PEMFCs. The RRDE technique reveals that the py-Fe–corrole/C favors a direct four-electron reduction pathway from O_2 to H_2O. The $H_2–O_2$ PEMFC using the py-Fe–corrole/C in the cathode outperforms Fe-based catalysts in previous studies, with greater durability and lower Fe loading. The high performance of the py-Fe–corrole/C can be attributed to the network structure of poly-aromatic hydrocarbons, the quaternary (graphitic)-type nitrogen and the coordination structure. Detailed SWV, *in situ* XANES and *in situ* EXAFS measurements were carried out to improve our understanding of the ORR with the py-Fe–corrole/C.

Acknowledgements

The authors would like to thank financial support from the Ministry of Education Top University Projects (100H451401), the National Science Council of Taiwan (NSC 101-2221-E-011-047-MY3), and the Academia Sinica.

Notes and references

1 Q. Liu, H. Zhang, H. Zhong, S. Zhang and S. Chen, *Electrochim. Acta*, 2012, **81**, 313–320.
2 Y. Hu, X. Zhao, Y. Huang, Q. Li, N. J. Bjerrum, C. Liu and W. Xing, *J. Power Sources*, 2013, **225**, 129–136.
3 H.-S. Oh and H. Kim, *J. Power Sources*, 2012, **212**, 220–225.
4 H.-J. Zhang, X. Yuan, L. Sun, J. Yang, Z.-F. Ma and Z. Shao, *Electrochim. Acta*, 2012, **77**, 324–329.
5 D. Zhao, J.-L. Shui, C. Chen, X. Chen, B. M. Reprogle, D. Wang and D.-J. Liu, *Chem. Sci.*, 2012, **3**, 3200–3205.
6 S.-T. Chang, C.-H. Wang, H.-Y. Du, H.-C. Hsu, C.-M. Kang, C.-C. Chen, J. C. S. Wu, S.-C. Yen, W.-F. Huang, L.-C. Chen, M. C. Lin and K.-H. Chen, *Energy Environ. Sci.*, 2012, **5**, 5305–5314.
7 H.-C. Huang, I. Shown, S.-T. Chang, H.-C. Hsu, H.-Y. Du, M.-C. Kuo, K.-T. Wong, S.-F. Wang, C.-H. Wang, L.-C. Chen and K.-H. Chen, *Adv. Funct. Mater.*, 2012, **22**, 3500–3508.
8 Y. Gao, T. r. Åkermark, J. Liu, L. Sun and B. r. Åkermark, *J. Am. Chem. Soc.*, 2009, **131**, 8726–8727.
9 A. Okamoto, R. Nakamura, H. Osawa and K. Hashimoto, *J. Phys. Chem. C*, 2008, **112**, 19777–19783.
10 J. Grodkowski, P. Neta, E. Fujita, A. Mahammed, L. Simkhovich and Z. Gross, *J. Phys. Chem. A*, 2002, **106**, 4772–4778.
11 K. M. Kadish, L. Fremond, Z. P. Ou, J. G. Shao, C. N. Shi, F. C. Anson, F. Burdet, C. P. Gros, J. M. Barbe and R. Guilard, *J. Am. Chem. Soc.*, 2005, **127**, 5625–5631.
12 D. K. Dogutan, R. McGuire and D. G. Nocera, *J. Am. Chem. Soc.*, 2011, **133**, 9178–9180.
13 P. Vasudevan, Santosh, N. Mann and S. Tyagi, *Transition Met. Chem.*, 1990, **15**, 81–90.

14 J. H. Zagal, *Coord. Chem. Rev.*, 1992, **119**, 89–136.
15 C. W. B. Bezerra, L. Zhang, K. Lee, H. Liu, A. L. B. Marques, E. P. Marques, H. Wang and J. Zhang, *Electrochim. Acta*, 2008, **53**, 4937–4951.
16 A. Serov, M. Min, G. Chai, S. Han, S. Seo, Y. Park, H. Kim and C. Kwak, *J. Appl. Electrochem.*, 2009, **39**, 1509–1516.
17 F. Jaouen, E. Proietti, M. Lefevre, R. Chenitz, J. P. Dodelet, G. Wu, H. T. Chung, C. M. Johnston and P. Zelenay, *Energy Environ. Sci.*, 2011, **4**, 114–130.
18 Z. Shi and J. Zhang, *J. Phys. Chem. C*, 2007, **111**, 7084–7090.
19 F. Beck, *J. Appl. Electrochem.*, 1977, **7**, 239–245.
20 J. P. Randin, *Electrochim. Acta*, 1974, **19**, 83–85.
21 L. Zhang, J. Zhang, D. P. Wilkinson and H. Wang, *J. Power Sources*, 2006, **156**, 171–182.
22 S. Baranton, C. Coutanceau, C. Roux, F. Hahn and J. M. Léger, *J. Electroanal. Chem.*, 2005, **577**, 223–234.
23 H. Alt, H. Binder and G. Sandstede, *J. Catal.*, 1973, **28**, 8–19.
24 Z. Chen, D. Higgins, A. Yu, L. Zhang and J. Zhang, *Energy Environ. Sci.*, 2011, **4**, 3167–3192.
25 A. Morozan, B. Jousselme and S. Palacin, *Energy Environ. Sci.*, 2011, **4**, 1238–1254.
26 D. S. Su and G. Sun, *Angew Chem., Int. Ed.*, 2011, **50**, 11570–11572.
27 A. A. Gewirth and M. S. Thorum, *Inorg. Chem.*, 2010, **49**, 3557–3566.
28 B. Koszarna and D. T. Gryko, *J. Org. Chem.*, 2006, **71**, 3707–3717.
29 C. A. Joseph, M. S. Lee, A. V. Iretskii, G. Wu and P. C. Ford, *Inorg. Chem.*, 2006, **45**, 2075–2082.
30 J. J. Rehr, R. C. Albers and S. I. Zabinsky, *Phys. Rev. Lett.*, 1992, **69**, 3397–3400.
31 C.-H. Wang, S.-T. Chang, H.-C. Hsu, H.-Y. Du, J. C.-S. Wu, L.-C. Chen and K.-H. Chen, *Diamond Relat. Mater.*, 2011, **20**, 322–329.
32 G. Lalande, R. Côté, G. Tamizhmani, D. Guay, J. P. Dodelet, L. Dignard-Bailey, L. T. Weng and P. Bertrand, *Electrochim. Acta*, 1995, **40**, 2635–2646.
33 J. M. Jiménez Mateos and J. L. G. Fierro, *Surf. Interface Anal.*, 1996, **24**, 223–236.
34 C.-H. Wang, H.-C. Hsu, S.-T. Chang, H.-Y. Du, C.-P. Chen, J. C.-S. Wu, H.-C. Shih, L.-C. Chen and K.-H. Chen, *J. Mater. Chem.*, 2010, **20**, 7551–7557.
35 H. T. Chung, C. M. Johnston, K. Artyushkova, M. Ferrandon, D. J. Myers and P. Zelenay, *Electrochem. Commun.*, 2010, **12**, 1792–1795.
36 G. Liu, X. Li, P. Ganesan and B. N. Popov, *Electrochim. Acta*, 2010, **55**, 2853–2858.
37 K. Lee, L. Zhang, H. Lui, R. Hui, Z. Shi and J. Zhang, *Electrochim. Acta*, 2009, **54**, 4704–4711.
38 J.-i. Ozaki, N. Kimura, T. Anahara and A. Oya, *Carbon*, 2007, **45**, 1847–1853.
39 T. Ikeda, M. Boero, S.-F. Huang, K. Terakura, M. Oshima and J.-i. Ozaki, *J. Phys. Chem. C*, 2008, **112**, 14706–14709.
40 H. Niwa, K. Horiba, Y. Harada, M. Oshima, T. Ikeda, K. Terakura, J.-i. Ozaki and S. Miyata, *J. Power Sources*, 2009, **187**, 93–97.
41 M. Manzoli and F. Boccuzzi, *J. Power Sources*, 2005, **145**, 161–168.
42 S. Pylypenko, S. Mukherjee, T. S. Olson and P. Atanassov, *Electrochim. Acta*, 2008, **53**, 7875–7883.
43 M. C. M. Alves, J. P. Dodelet, D. Guay, M. Ladouceur and G. Tourillon, *J. Phys. Chem.*, 1992, **96**, 10898–10905.
44 N. Ramaswamy and S. Mukerjee, *Adv. Phys. Chem.*, 2012, **2012**, 17.
45 T. M. Arruda, B. Shyam, J. S. Lawton, N. Ramaswamy, D. E. Budil, D. E. Ramaker and S. Mukerjee, *J. Phys. Chem. C*, 2009, **114**, 1028–1040.
46 T. M. Arruda, B. Shyam, J. M. Ziegelbauer, S. Mukerjee and D. E. Ramaker, *J. Phys. Chem. C*, 2008, **112**, 18087–18097.
47 M. Teliska, V. S. Murthi, S. Mukerjee and D. E. Ramaker, *J. Electrochem. Soc.*, 2005, **152**, A2159–A2169.
48 M. Teliska, W. E. O'Grady and D. E. Ramaker, *J. Phys. Chem. B*, 2005, **109**, 8076–8084.
49 J. M. Ziegelbauer, T. S. Olson, S. Pylypenko, F. Alamgir, C. Jaye, P. Atanassov and S. Mukerjee, *J. Phys. Chem. C*, 2008, **112**, 8839–8849.
50 H. Schulenburg, S. Stankov, V. Schunemann, J. Radnik, I. Dorbandt, S. Fiechter, P. Bogdanoff and H. Tributsch, *J. Phys. Chem. B*, 2003, **107**, 9034–9041.
51 M. Lefevre, J. P. Dodelet and P. Bertrand, *J. Phys. Chem. B*, 2002, **106**, 8705–8713.
52 M. Lefèvre, J. P. Dodelet and P. Bertrand, *J. Phys. Chem. B*, 2000, **104**, 11238–11247.
53 A. L. Bouwkamp-Wijnoltz, W. Visscher, J. A. R. van Veen, E. Boellaard, A. M. van der Kraan and S. C. Tang, *J. Phys. Chem. B*, 2002, **106**, 12993–13001.
54 M. Bron, J. Radnik, M. Fieber-Erdmann, P. Bogdanoff and S. Fiechter, *J. Electroanal. Chem.*, 2002, **535**, 113–119.